Remote Sensing of Laterized Archaean Greenstone Terrain: Marshall Pool Area, Northeastern Yilgarn Block, Western Australia

S. A. Drury and *G. A. Hunt*
Department of Earth Sciences, The Open University, Milton Keynes MK7 6AA, United Kingdom

ABSTRACT: Airborne multispectral image data, equivalent to those from the Landsat-5 Thematic Mapper, are tested over an intractible terrain of deeply lateritized Archaean basic and ultrabasic igneous rocks that can normally only be mapped by intensive field work backed up by rotary air-blast drilling. The most appropriate combinations of bands to express the bulk of geological information in the data as false-color images are 7, 5, 4 and 7, 4, 2 in red, green, blue order. The high interband correlation inherent in the reflected part of the spectrum, which normally results in bland false-color images, can be overcome to some extent by the use of decorrelation stretching of the bands. This produces images which successfully discriminate all the major lithologies in the area from each other and from superficial deposits. The discrimination is essentially empirical because of the complex nature of the surfaces involved and the breadth of the bands. Consequently, it is difficult to rationalize the results in terms of the spectral effects of different components of the local soils, clasts of bedrock, and vegetation. Nevertheless, the results are consistent over large areas and promise improved pace and accuracy of geological mapping in the Archaean greenstone terrains of Australia, now that Landsat Thematic Mapper data have become routinely available since the airborne survey was completed.

INTRODUCTION

The Yilgarn Block of Western Australia forms one of the world's largest continuous areas of Archaean crust. As well as being structurally complex and lithologically diverse, it is an area of unremitting low relief and has suffered deep lateritic weathering. It is a difficult area to map by conventional field methods, and many problems of structure and petrogenesis remain to be solved. In these respects it is unlike many of the areas previously examined in a geological context by remote sensing (eg., Podwysocki *et al.*, 1983; Abrams *et al.*, 1984; Bird *et al.*, 1985; Sultan *et al.*, 1987). Intractible terrains of this kind are common at low latitudes, and allow the geological usefulness of imagery to be tested to the limit.

Marshall Pool is about 70 km northwest of Leonora, in an area of semi-desert (rainfall 200 mm yr^{-1}), with subdued relief (400 to 500 m). Most of the relief coincides with areas of float-rich colluvium around sparse outcrop, or with residual caps of laterite duricrust. Alluvium derived from this forms wide, featureless plains laced with ephemeral drainage channels, recognizable only by their associated trains of denser vegetation. Except after unusually wet seasons, the soil is bare of ground-hugging grasses and flowering plants, and the dominant vegetation is a sparse cover (<10 percent) of *Acacia* and various salt tolerant shrubs, with rare *Eucalyptus* along drainage courses. The main agent of erosion is sheet flooding. The sparse cover and needle-like leaves of sclerophyll vegetation make the canopy almost transparent to incident radiation, and the only effect on images, outside drainage channels, is a slight decrease in albedo, due to shadowing. The appearance of multispectral images, therefore, is directly controlled by variations in the surface composition of soil, float, and outcrop.

Here we examine the potential of airborne, broad-band image data in the visible, very-near infrared (VNIR), and short-wavelength infrared (SWIR), which are equivalent to those available for Australia from the Landsat Thematic Mapper (TM) since mid 1987. We concentrate on the use of likely spectral features in weathered rocks and lateritic soils to select combinations of bands and interband ratios to display in color, and on means of overcoming the high interband correlations which often produce muted color images. Geological maps from the TM-equivalent images are compared with conventional maps derived by intensive field work and interpretation of natural-color aerial photographs.

GEOLOGY

Hallberg (1986) has subdivided the Archaean terrain of the Leonora-Laverton area into several "tectonic zones" and "geological sectors," based on structural and stratigraphic evolution. The Keith-Kilkenny Tectonic Zone, part of which is examined here, runs northwest from Leonora, and is characterized by intense, probably oblique-slip shearing along features such as the Mount George-Clifford shear belt (Figure 1) and earlier isoclinal folding of a bimodal suite of Archaean supracrustal lithologies. This comprises an ultrabasic-basic suite of lavas and associated intrusions, and various silicic volcanoclastic sediments formed on the flanks of rhyodacitic volcanic centers. The stratigraphic sequence and most primary structures are disrupted by the heterogeneous deformation in shear belts. The tectonic zones are flanked by less complex geological sectors, characterized by open upright folding and relative continuity of stratigraphy. In the Murrin-Margaret Geological Sector to the east, a lower sequence of basic volcanics with quartzose sediments is succeeded by an association of ultrabasic-basic volcanics and quartz-poor feldspathic sediments derived from andesitic volcanic centers.

The structural evolution of the Keith-Kilkenny Tectonic Zone had four distinct components. Early structures are isoclinal folds with axial traces parallel to regional strike, one of which – the Hangover Synform – forms the focus of this study. There are signs that even earlier folds may be refolded by these structures (see below). In the Mount Ross and Mount Fouracre areas, the isoclines are clearly refolded by upright structures, so that their axial traces are sinuous, ranging from NNW-SSE to E-W within the tectonic zone. The areas where isoclinal folds and later refolding structures are clearly seen are on the flanks of several major shear belts, the most prominent of which is the Mount George-Clifford shear belt (Figure 1). Compositional layering and earlier folds are rotated into the NW-SE shear belt and become extremely drawn out, possibly defining a system of sheath folds. Easily recognized primary lithologies and struc-

Photogrammetric Engineering and Remote Sensing,
Vol. 54, No. 12, December 1988, pp. 1717–1725

0099-1112/88/5412–1717$02.25/0

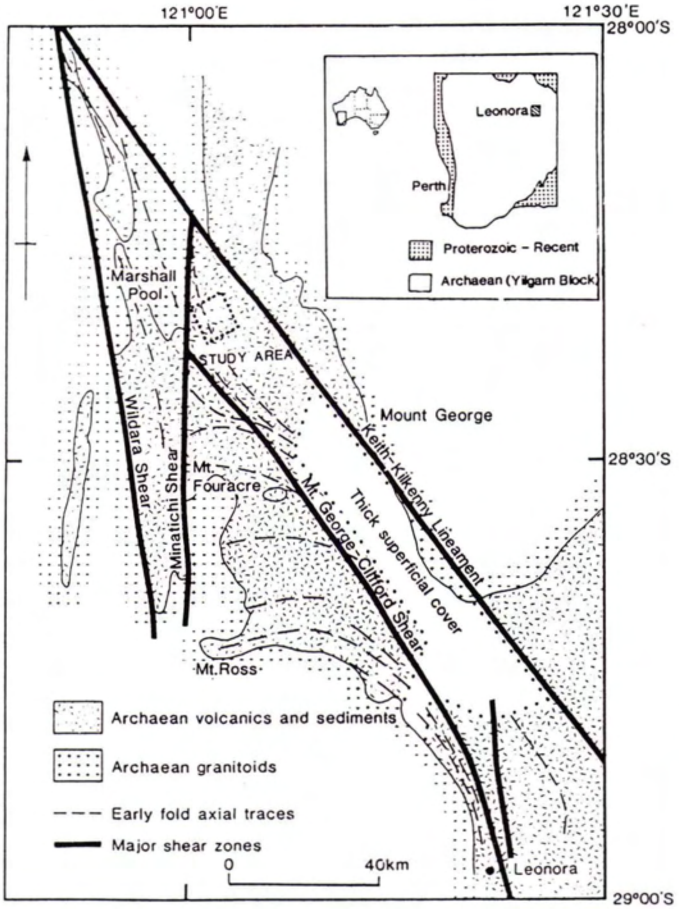

FIG. 1. Regional structure of the eastern part of the Leonora 1:250 000-scale map sheet (Thom and Barnes, 1977, Figure 2).

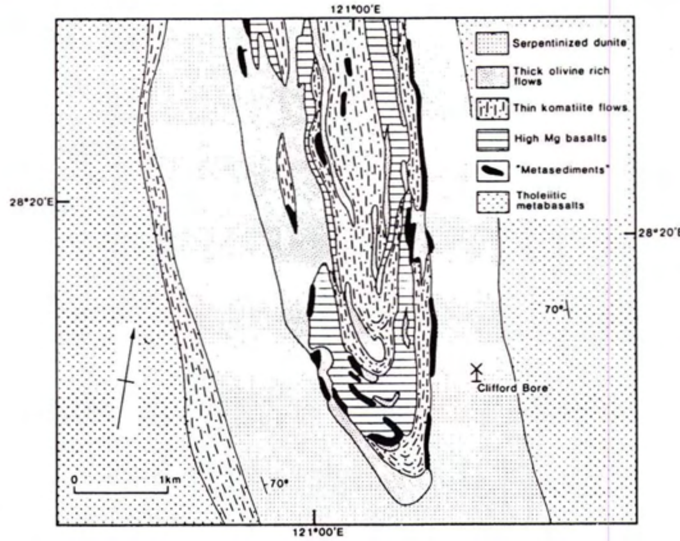

FIG. 2. Geology of the Hangover Bore area (Donaldson, 1982).

tures in the areas of low strain are completely disrupted, and only the broadest compositional divisions can be recognized in the schists which characterize the shear belt. The youngest Archaean lithologies in the Keith-Kilkenny Tectonic Zone are polymict conglomerates containing granitoid clasts, which appear to fill a graben-like feature associated with late extensional tectonics (Hallberg, 1986).

The area studied around the Hangover Synform has been extensively explored for primary nickel mineralization in ultrabasic lavas and associated intrusions, and comprises a zone of outcrop and colluvium in a low strain part of the Keith-Kilkenny Tectonic Zone. It is particularly useful for a test of TM data over lateritic colluvium and outcrop because it is lithologically diverse in a zone of low strain, has been well mapped by use of rotary air-blast drilling and contact mapping by Donaldson (1982) (Figure 2), and has natural-color aerial photograph cover at a scale of 1:25 000. In structurally upward sequence the main lithologies folded by the Hangover Synform are thick pillowed metabasalts, a serpentinized dunite, a stratigraphically complex sequence of komatiites, high-MgO metabasalt and olivine-rich peridotite flows, and a core to the synform of thin komatiite flows with olivine-rich layers. The sequence in the synform core also contains discontinuous patches of intraflow sediments. Our field work indicates that the high-MgO metabasalt may have been misidentified, at least in part. The float which we examined during traverses across this unit is gabbroic in texture, but is magnesian and deficient in feldspars. We were unable to locate any of the small outcrops of metasediments.

LATERITIZATION

The peneplane of the Yilgarn Block is at least Permian in age, and the fact that its surface is close to the projection of the surrounding Proterozoic unconformity suggests that it may have been initiated as much as 1100Ma ago (Gee *et al.*, 1981). From the early Cretaceous to mid-Eocene, a warm humid climate supported rain forest extending to the center of the Australian continent. During this time a high water table and massive production of humic acids rotted bedrock to as much as 100 m deep (McFarlane, 1976; Fitzpatrick, 1980). Above the weathering front, rock-forming minerals were altered to a variety of secondary products, summarized by Table 1, dominated by clay minerals and various iron oxides and hydroxides. This vertical mineralogical zonation, together with leaching of soluble components, produced the typical laterite profile (Figure 3), enriched in its upper parts by less-mobile secondary compounds of Fe, Al, Si, and Mn, and resistant minerals such as zircon and chromite. Quartzofeldspathic rocks have developed profiles rich in kaolinite, quartz, and secondary silica, whereas basic and ultrabasic lithologies show a higher proportion of secondary iron minerals in the laterite soil (Butt, 1981, 1983). In both cases, the concentration of Fe and Mn compounds at the former water table formed the pisolitic duricrust, which is the most easily recognized aspect of lateritic profiles. The low primary Al content of some ultrabasic rocks reduces the formation of clay minerals in the profile, so that silica released by breakdown of ferromagnesian silicates is retained in uncombined form as chalcedony and opal to form a major component of the laterite profile (Figure 3).

The present relief in the Yilgarn stems from the incision and erosion of the laterite profile towards the close of the pluvial period in the Miocene, a process that has slowed as conditions became more arid (Ollier, 1978). The major elements of drainage, now delineated by strings of large playas, date from this time. In the study area, the laterite duricrust forms isolated plateaux, or "breakaways," between which the profile has been eroded down to the level of the saprolite zone and in many cases to the oxidized bedrock. It is to the dominant mineralogies of these zones that the remote senser must look in order to exploit the full potential of multispectral image data. Remote-sensing strategy depends on lithologically determined variations of clay minerals, secondary silica, magnesite, and ferric minerals in lateritic soils, and to a lesser extent on the more

TABLE 1. WEATHERING PRODUCTS OF ROCK-FORMING MINERALS AT DIFFERENT ZONES IN LATERITE PROFILE. FOR EACH COLUMN, THE SEQUENCE OF NEW MINERAL FORMATION IS FROM BOTTOM UPWARDS.

Ferruginous duricrust	gibbsite + kaolinite				haematite goethite	
Pallid or mottled clay zone	kaolinite	kaolinite	kaolinite	smectite kaolinite	haematite goethite	
Saproline zone			kaolinite smectite	smectite kaolinite	haematite goethite	kaolinite
Oxidised rock zone	sericite	vermiculite montmorillonite	chlorite vermiculite smectite	smectite vermiculite chlorite	martite	illite mont-mor-illonite
Fresh rock zone	feldspars	Felsic rocks hornblende, biotite	Basic rocks amphiboles, pyroxenes	Ultrabasic rocks olivines, pyroxenes	magnetite	clay minerals

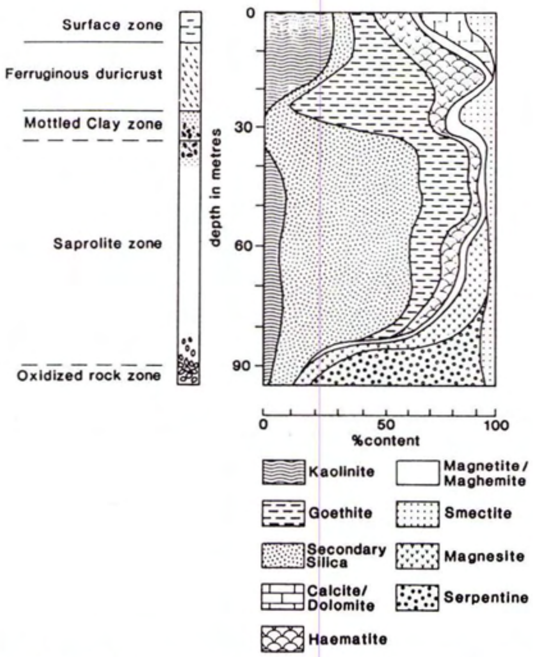

FIG. 3. Division and mineralogy of a laterite profile developed on ultrabasic rocks near Kalgoorlie, Western Australia (Smithh, 1977).

resistant primary silicates such as chlorite, talc, and serpentines in float fragments.

Outside the areas of net erosion, where products of laterite weathering and fragments of rock (float) relate directly to underlying lithologies, the surface is coated with variable thicknesses of transported lag gravels. Most prominent among these are black limonitic pea gravels eroded from duricrust and white quartzite gibber derived from quartz veins. Due to the resistance of quartzite fragments under prevailing climatic conditions, the latter give a disproportionate impression of the importance of quartz veining in an area. In areas of lag gravels, mapping of bedrock lithofacies and structure is impossible by any technique except drilling. In areas of untransported colluvium, variations in composition and petrographic texture of float fragments allow moderately detailed lithofacies maps to be made by conventional mapping techniques, although the paucity of true outcrop precludes quantitative structural mapping. The pervasive iron and manganese staining of float and soil in areas of colluvium masks the lithological diversity to both the human eye and to the camera, the only differences in the visible and VNIR being due to albedo in a red-hued terrain. Consequently, photogeology is a poor guide to lithology, though of some use in exploiting the structurally controlled attributes of the subdued topography (see below).

REMOTE SENSING STRATEGY

Figure 4a shows visible and VNIR spectra of some important ferric oxides and hydroxides. Charge-transfer absorptions in the visible determine the perceived color differences between haematite (red), goethite (yellow-brown), and limonite (orange-brown). Using TM bands 1, 2, and 3 (natural-color components) should allow some discrimination between surfaces stained by these species, although confusion is possible through mixing with others. Given narrow-waveband data, the Fe^{3+} crystal-field absorption feature in the 840 to 920nm region could be exploited. However, the breadth of TM band 4 suggests that all that can be expected is detection of the presence of ferric minerals and non-unique estimates of their abundance from the depth of the absorption feature.

Figure 4b gives an impression of the possibilities for discrimination among hydroxylated silicates and aluminosilicates, carbonates, and sulphates in the SWIR. Unfortunately, none of the unique intricacies can be spectrally resolved by TM band 7. All that is possible is the empirical use of the differences between the reflectance high (1550 to 1750nm, TM band 5) and lows due to sulphates and hydroxylated silicates in TM band 7. The absorption feature in carbonates is too close to the edge of the band 7 bandpass to have any noticeable effect on radiance.

Quartz and secondary silica have no spectral features due to molecular structure in the SWIR, and because of this should be discriminable from hydroxylated silicates. The high mechanical water content of opaline silica and chalcedony should be revealed by strong absorption in the 1400 and 1900nm wavebands, thereby depressing reflectance in the SWIR compared with the normally high albedo of these minerals. A similar decrease in SWIR reflectance can be expected for serpentines, because of the relatively higher opaque-mineral content which "quench" visible to SWIR spectal features (Hunt *et al.*, 1981).

The multispectral data available to us is from an aerial survey by Hunting Geology and Geophysics in January 1984, using a Daedalus AADS 1268 11-band scanner. We selected bands

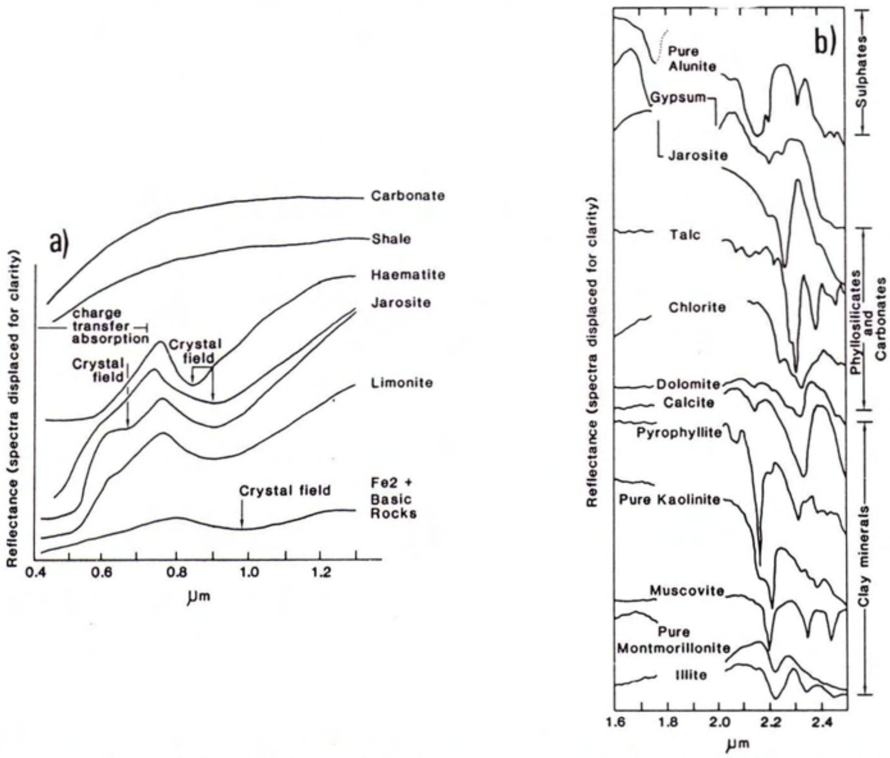

FIG. 4. (a) Visible and VNIR spectra of iron minerals, (b) SWIR spectra of some metamorphic minerals and products of weathering (J. Huntington, CSIRO, *pers. comm.*, 1986).

corresponding to those available from Landsat TM (1. 450 to 520 nm, 2. 520 to 600 nm, 3. 630 to 690 nm, 4. 760 to 900 nm, 5. 1550 to 1750 nm, 7. 2080 to 2350 nm, 6. 8500 to 13000 nm). The flying height of 8000 m and IFOV of 2.5 mrad gave a pixel size of approximately 15 m. The 86° field of view leads to some panoramic distortion across each data swath, but this was corrected during preprocessing. No further geometric correction was attempted because accurate large-scale maps are unavailable for this area. Although some cross-track shading (Gerstl and Simmer, 1986) is probably present in the data, it is not immediately apparent, even on images with extreme contrast stretches. No attempt was made to correct for this common defect of airborne data.

Ground truth comprised a geological map prepared by Western Mining Corporation Ltd, during protracted nickel exploration in the area (Donaldson, 1982), natural-color aerial photographs at 1:25 000 scale supplied by Esso Minerals Ltd, and five detailed sampling traverses by ourselves.

The strategy for digital image processing of the Daedalus data had two components. First, the best combination of bands to present as a single false-color composite, and to combine in color-ratio composites, is selected. Second, means to overcome the problem of interband correlation that characterizes all data from the reflected part of the spectrum, and results in bland false-color composites, are sought. An important consideration for future use of operational TM data was to suggest methods that balance optimum geological usefulness with a minimum of processing time and as few final image products as possible. There is often a temptation in digital image processing to generate large numbers of different images, many of which only add marginally to the effectiveness of a few key types.

Finding the optimum combination of three bands to display as red, green, and blue components of a color image by trial and error becomes more confusing as the number of available bands increases. For seven bands there are 210 permutations. There are two kinds of approach using multispectral statistics from training areas. A correlation coefficient matrix allows the construction of tie-line and cluster diagrams (Hunt *et al.*, 1986), which highlight the least and most highly correlated bands in a data set. The most informative three bands are the least well correlated. Sheffield (1985) claims that ranking three-band combinations according to the determinants of their 3 by 3 variance-covariance matrix within seven-dimensional data space is a more rigorous method. The determinant is a measure of the volume of the three-band ellipsoid, and relates to the entropy of the multispectral image. The "best" combination has the highest of all possible volumes. Even using training areas biased towards known areas of colluvium does not distinguish between geological and non-geological information in the data. For instance, band 1 figures in four of the top six ranked combinations because it contains more effects due to atmospheric scattering than other bands. Band 4 occurs in each of the top four, suggesting that it is highly discriminating in poorly vegetated terrain, probably due to the fact that it contains the Fe^{3+} crystal-field absorption. Bands 6 and 1 dominate the lowest ranked combinations, indicating that both have high variance and are affected by atmospheric effects, and are thereby of little use in three-band images. Because the geological information in the data over such spatially and spectrally subdued terrain forms a minor component in the data set, subjective selection relying on known spectral features of rocks and minerals, and on field knowledge, are important adjuncts to objective selection of band combinations.

Bands 1 to 4 contain information on iron minerals and vegetation – the Fe-O charge-transfer feature in band 1, an Fe^{3+} reflectance ramp from band 2 to 3, the "red edge" from 3 to 4, and the Fe^{3+} crystal-field absorption in band 4. Bands 5 and 7 provide evidence on the presence of hydroxylated phyllosilicates – the reflectance peak of clay minerals in band 5 and the diverse Al-OH and Mg-OH absorption features in band 7. Band 5 is also on the shoulder of the 1450-nm water absorption feature, and should indicate variations in mechanical water content in opaline silica and serpentines. Because we had no data on thermal properties of local soils and band 6 was of poor quality due to atmospheric effects, band 6 was rejected from further use. Band 1 was also rejected because of poor dynamic range, leaving five bands to consider. Of these, bands 2 and 3 are very highly correlated and span the same Fe^{3+} reflectance ramp, so one could be dropped from the analaysis. Band 2 was chosen, because it spans more of the Fe^{3+} transopaque region than band 3. By reducing the number of bands to the four likely to reveal the most geological information, instead of 210 possible RGB (red-green-blue) permutations, only 24 had to be considered. By visual inspection, the most useful combination for the Marshall Pool area was bands 7, 5, and 4. Because human chromatic vision is increasingly efficient at perceiving small differences in hue in the order green, red to blue (Canas and Barrett, 1985), the band likely to contain most geological information in lateritic terrains, i.e., band 4 (iron content) controls blue, band 7 (phyllosilicates) is assigned to red, and band 5, with the simplest geological "message" (albedo and water content), controls green. This rendition, after interactive contrast stretching, is shown for the area in Plate 1a. Another effective rendition from the chosen four bands, combining bands 7, 4, and 2 as RGB, is shown in Plate 1b. The interesting feature from comparison of these two images is that the 7,5,4 image is more geologically discriminating than that of 7,4,2, yet the first is ranked eighth by Sheffield's (1985) objective method and the latter third.

Both Plate 1a and 1b, although moderately colorful, do not exploit RGB color space fully, due to the inherent correlation between bands in the reflected part of the EM spectrum. A frequently used means of overcoming this hindrance to interpretation is principal component analysis of the multispectral data, based on the variance-covariance matrix of the whole scene (Soha and Schwartz, 1978). The data from N bands are combined additively, after weighting by the eigenvectors associated with each principal component and band, to produce a decorrelated spread on N orthogonal principal component axes. After suitable stretching of the principal components, the data now fill the N-dimensional space much more fully.

Displaying principal components in RGB or other color spaces gives a rendition which exploits color to the limits permitted by the data. This is extremely useful in identifying arbitrary boundaries on the imagery. However, the method suffers from several important drawbacks. Because increasing order principal components have progressively lower signal-to-noise ratios and yet are equally weighted in the image, the image is very noisy and much textural information is lost to the interpreter. It is difficult to interpret the spectral contribution of different types of surface to colors on the image, because each component is a weighted additive combination of all bands. The eigenvectors used to weight each band in assembly of each component are very sensitive to the multispectral covariance statistics of the scene, and the rendition varies widely from subscene to subscene, and from date to date.

After stretching principal components to fill N-dimensional space more fully, it is possible to restore the data to the original band axes simply by adding stretched principal components weighted by the inverse of the eigenvector matrix. Because each restored band axis incorporates elements of the decorrelation inherent in principal component analysis, this is known as a *decorrelation stretch* or *D-stretch* of the band data (see Gillespie *et al.*, 1987). The resulting images retain the original hues, which are to some extent predictable from the spectral properties of the surface, but have stretched intensity and saturation that are impossible by interactive means. Plates 2a and 2b are the D-stretched band 7, 5, 4 and 7, 4, 2 images used by us for the bulk of interpretation in the Hangover Bore area.

Band ratioing techniques are aimed at emphasising the spectral differences between different surfaces. The numerator and denominator bands are generally chosen to express the radiance differences in bands related to a particular spectral feature (Table 2). In this case, ratios were chosen to enhance hydroxylated sheet silicates, and Fe^{3+} and Fe^{2+} features (ratios 7:5, 4:2, and 5:4). Ratios add so little geological information to that derived from D-stretched three band images that they are not discussed further.

DISCUSSION OF RESULTS

Figure 2 represents the main base for comparison between different methods of geological mapping, and resulted from interpretation of aerial photographs, contact mapping of float and sparse outcrop, and numerous east-west rotary air-blast drilling traverses spaced at roughly 100-m intervals (Donaldson, 1982). Considering the poor exposure, it is quite detailed.

Figure 5 is our interpretation without field control by stereoscopic examination of 1:25 000-scale natural color aerial photographs, presented at the same scale as Figure 2 and Plates 1 and 2. The photographs express the very limited tonal range of the terrain as well as possible by photographic methods. They are mainly reddish browns variably mixed with grey-green speckle due to local soil control over vegetation density. The information content is little better than that contained in minus-blue panchromatic photographs. Vertical exaggeration of the subdued relief helps outline the gross variation in strike of boundaries between units of subtly different resistance, which helps highlight possible early isoclinal fold closures in the western limb of the synform. Together with tonal differences in soil and vegetation cover, relief helps distinguish 4 categories of surface shown in Figure 5. Surface type 1 is pale grey tinged with orange and has low vegetation cover, except in drainage courses. It is resistant relative to type 2. Type 2 is light orange-brown with low to very low vegetation cover, and has low resistance to erosion. Type 3 is greenish grey due to moderate vegetation cover, tinged with light orange-brown soil. It is resistant compared with type 2. The boundaries of these three surface categories correspond to some of the geological boundaries on Figure 2. The fourth type is irregularly distributed and oversteps the geological boundaries, corresponding to areas of sheetwash and thick, disturbed laterite. It is an irregularly mottled mixture of colluvial material derived from laterite cap and pallid zone, plus pisolitic lag gravels.

One of these surface types (1) includes the unit of thin komatiite flows in the core of the synform, comprising olivine-rich cumulates and metasediments, distinguished on Figure 2. It also includes thin discordant bodies of xenolith-rich dolerite that have not been mapped previously (D on Figure 5). The komatiite unit mapped on the eastern limb is covered by type 2, together with the high-MgO and tholeiitic metabasalts of Figure 2. Surface type 3 corresponds fairly closely to the thick serpentinised dunite of Figure 2, and is the only photogeological unit which is well correlated with lithology.

Compared with the natural-color aerial photographs, the images of Daedalus SWIR and visible data (Plate 1) are better means of lithological discrimination, though the textural detail is much lower due to the inferior resolution. This discrimination is dramatic in the D-stretched versions (Plate 2). Table 3 summarizes the colors associated with the main lithological units and other elements of the terrain.

Although, on Plate 2a, there is confusion between the hues of olivine-rich cumulates and vegetation, they are easily discriminated in most cases by context, ie. the vegetation is clearly associated with drainage features as narrow, irregular ribbons. The olivine-rich cumulates are uniquely expressed in cyan on Plate 2b. Both units field mapped as komatiite are expressed

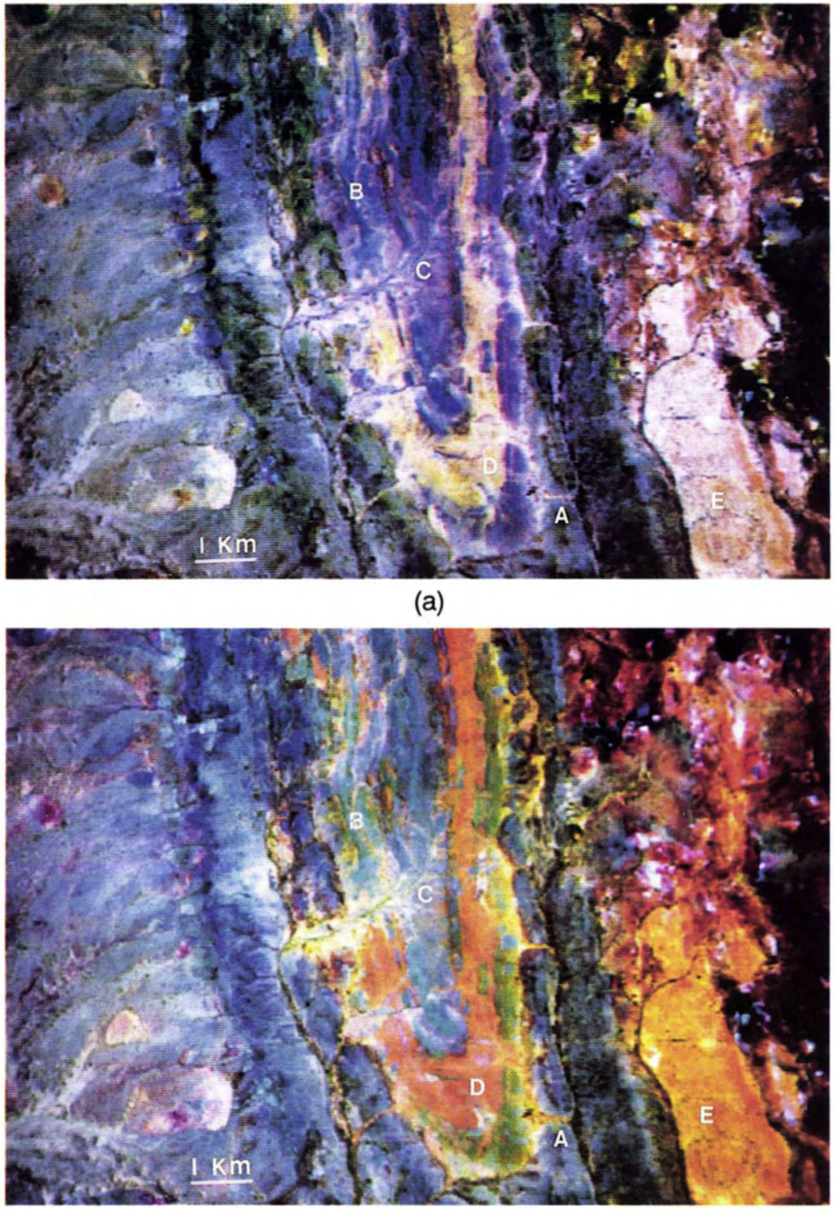

(a)

(b)

PLATE 1. (a) Image of TM bands 7, 5, and 4 displayed as red, green, and blue for the Hangover Synform; (b) bands 7, 4, and 2 as RGB. Letters refer to lithologies on Figure 6 and in Table 3.

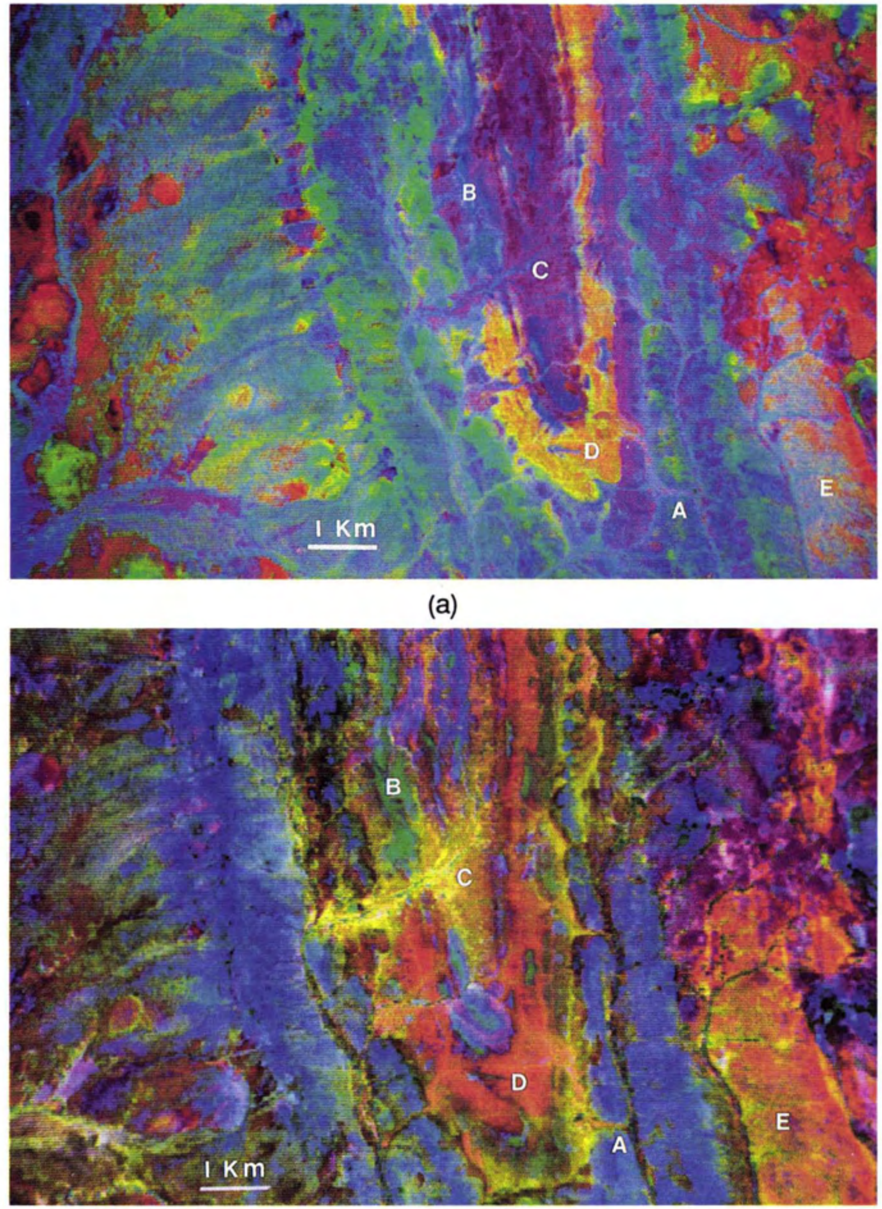

(a)

(b)

PLATE 2. As Plate 1, but data have been enhanced by decorrelation stretch (see text). Letters refer to lithologies on Figure 6 and Table 3.

TABLE 2. COMMON RATIOS USED IN DISCRIMINATION OF SURFACE TYPES

Numerator	Denominator	Application
7	5	Argillic vs. non argillic
3	4	Rocks vs. vegetation
5	1	Fe^{3+} vs. Fe^{3+} free
5	4	Argillic vs. Fe^{2+}
4	2	Fe^{2+} vs. non Fe^{2+}

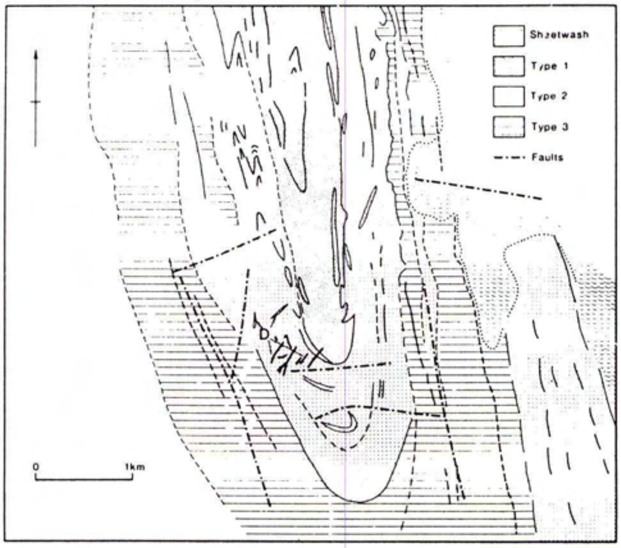

FIG. 5. Photogeological interpretation of the Hangover Synform based on 1:25 000-scale natural color aerial photographs, showing structural form lines and areas with different tone/texture characteristics.

TABLE 3. COLORS ASSOCIATED WITH DIFFERENT FIELD-MAPPED UNITS. LETTERS REFER TO LITHOLOGIES MAPPED ON PLATES 1 AND 2 AND FIGURE 6.

Material	Color on 7, 5, 4 (Plate 2a)	Color on 7, 4, 2 (Plate 2b)
Vegetation	blue	green
Superficials	orange-red green and magenta	orange-red
A. Dunite sill	green or dark magenta	green-blue
B. Olivine cumulates	blue	cyan
C. Thin komatiite flows	magenta	lilac or green-yellow
D. High-MgO gabbro (?)	yellow	orange-red
E. Tholeiite	pale lilac	orange-red

identically on Plate 2a, but there is confusion with elements of the superficial veneer in the west-central part of the image. This confusion is not present on Plate 2b and, moreover, the two komatiite units are clearly distinct from one another. Of all the lithologies, the high-MgO gabbro is most sharply and uniquely discriminated in bright yellow on Plate 2a. The same unit appears orange-red on Plate 2b and is confused with parts of the superficial veneer and the tholeitic metabasalt. The last is quite distinct on Plate 2a. Of all the bedrock units, the dunite sill is least well discriminated in Plate 2, having essentially the same range of hues as parts of the superficial veneer. That it stands out at all is due to its division into a number of color bands that parallel the strike of the better discriminated lithologies. These feature are best seen on Plate 2a as green and magenta bands on the eastern limb of the synform. None of the outcrops of the metasedimentary units in the area manifest themselves on either image. However, the dolerite dykes shown by the aerial photographs can be discerned as thin reddish streaks on Plate 2a, though whether they would have been noticed without prior knowledge of their existence is questionable.

The empirically derived conclusion from these observations is that the two selected band combinations of Daedalus data contain far more lithologically discriminating information than natural color photographs. However, even with a decorrelation stretch, neither image alone expresses the full information content. Using both images enables all major lithologies except metasediments to be discriminated clearly. Small metasediment patches indicated on Figure 2 are not discernible on aerial photographs and are difficult to locate in the field. Two different kinds of surface can be distinguished for both komatiites and the dunite sill. On the field and petrographic evidence that we have, it is not yet possible to verify that these image differences reflect significant differences in lithology.

Despite being an order of magnitude poorer in resolution, the D-stretched 7, 5, 4 and 7, 4, 2 images are equally as efficient at outlining large structural features as aerial photographs of the Marshall Pool area. This is because subtle differences among the volcanic flows and within the concordant intrusions are more strongly contrasted in a greater variety of hues. The better resolution of the aerial photographs only helps reveal local structural complexities at sharp lithological contacts and in exposed finely banded units.

Figure 6 is a geological map made by interpreting Plates 2a and b. Rather than outlining individual small areas with arbitrarily selected different colors, to produce an "objective" map of surface categories, connections and interpolations are made on the basis of general geological "rules" and our limited amount of field work. Solid and dashed geological boundaries represent subjectively those to which higher and lower confidence are attached. The map differs in several details from that in Figure 2, noteably the absence of a major olivine-rich flow from the western limb of the synform, the lack of continuity of the high-MgO unit on the west limb, and the inference of several faults.

Seeking explanations for the colors associated with the different lithologies on Plates 1 and 2 is difficult. The surface within an individual pixel of Daedalus data is generally a mixture of silt- to gravel-size soil, variable proportions of cobbles of float, and variable cover of sclerophyll shrubs. The soil itself may comprise varying proportions of products of lateritic weathering

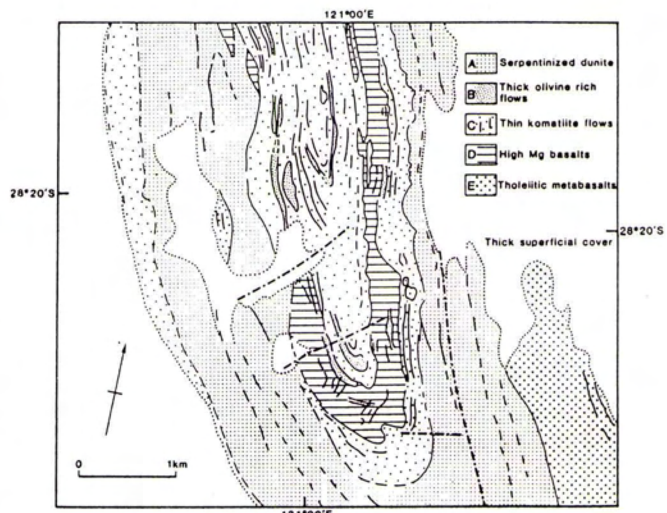

FIG. 6. Geological map based on information from Plate 2 and three traverses across strike.

– limonite, clays, and opaline silica – grains of unaltered minerals from the underlying bedrock and varying amounts of carbonate or silica cement. Surfaces on the cobbles of float are mixtures of iron and, to a lesser extent, manganese oxide patina with variably altered primary minerals. The latter may consist of anhydrous igneous minerals such as feldspars, pyroxenes, and olivine or hydroxylated products of metamorphism, such as chlorite, serpentines, talc, and epidote. The influence of vegetation on spectral response from a pixel is a combination of shadowing effects and a contribution of the species' particular spectral characteristics. In short, the spectral reflectances from Daedalus pixels are mixtures derived from many components. A further complicating factor, which virtually rules out any rigorous attempt to separate different spectral contributions to images, is the broad nature of the Daedalus and TM wavebands. All that can be attempted is to assess major contributing spectral factors in terms of their average reflectance across the bands in question.

The blue and green color of vegetation in drainage channels on Plates 2a and b, respectively, is due to the high reflectance in band 4 by plant cells, absorption by chlorophyll in band 2, and reflectance lows in bands 5 and 7 due to the relatively high water content of vegetation.

The olivine-rich cumulates, which appear blue and cyan on Plates 2a and b are usually associated with very low vegetation cover, and form tracts of pale grey float with little weathering patina. Consequently, they have high visible to very-near infrared albedo. Their coloration on Plates 2a and b suggests low band 7 and 5 relative to 4 and 2. This is possibly due to their high content of serpentine minerals, whose non-structural water content will lead to strong absorption around 1400 and 1900 nm, thereby decreasing reflectance in bands 5 and 7.

The komatiites, which appear magenta on Plate 2a, and both pale lilac and green on Plate 2b, preserve much of their primary igneous mineralogy and texture in float. The soil contains up to 10 percent magnesite and is only sparsely vegetated. The bulk reflectances in bands 7 and 4 must be higher than in band 5, to explain the magenta color in Plate 2a. For most minerals, band 5 represents a reflectance peak. The only common mineral that has a lower reflectance in band 5 than band 4 is talc (our unpublished data). However, talc also has a very low bulk reflectance in band 7, so that to explain the relatively high band 7 reflectance of komatiites and their color in Plate 2a requires the presence of other minerals in the soils mixed with the talc.

The tholeiitic metabasalts appear pale lilac to cream on Plate 2a and orange on Plate 2b. This implies high reflectances in bands 7, 5, and 4 and low in band 2. Our unpublished spectra for chloritic metabasalts from elsewhere in Western Australia have such characteristics, suggesting that the unique signature of tholeiites in Figure 5 is probably due to the high content of chlorite revealed in thin sections of these fine-grained pillow lavas.

The most distinctive unit on Plate 2a is the high-MgO gabbro, with a vivid yellow color. On Plate 2b it appears orange-red and is confused with tholeiites. This implies high band 7 and 5 and low band 4 and 2 reflectances from each mixed pixel. The unit has very sparse vegetation cover and a uniform texture on aerial photographs, so that it should be a simple matter to account for its coloration. Although the soil contains a high proportion of float and is strongly iron stained, a very common mineralogical component is opaline silica, formed in the laterite profile over this lithology. This has the requisite broad spectral features to explain the high contribution of bands 7 and 5 to image color (our unpublished data). The dominance of ferric iron minerals in the soils and patinas around float fragments would explain relatively low band 4 and lower still band 2 reflectances.

The largest homogeneous unit mapped in the area is the dunite sill (Figure 2). On Plate 2a parts of it appear green and others dark purple. These features indicate bulk spectral reflectances in the Daedalus bands as follows: low 7, high 5, low 4; higher 7 and 4 than 5, respectively. The unit is virtually unexposed, much of the surface being an iron-rich mottled zone of the laterite profile containing no float. The color banding is not due to variations in vegetation density, which, although at its highest for the area, maintains a uniform cover and no variation that we noticed in species density. The green bands on Plate 2a correlate exactly with mottled zone material. Goethite and hematite, both of which are present at the surface, have low band 4 reflectances relative to those for 5 and 7, due to a strong Fe^{3+} crystal-field feature around 880 nm. The observed low band 7 reflectance may be due to a high proportion of clay minerals in the mottled zone. The dark purple band is found at slightly lower elevation, and may reflect erosion through the mottled zone to reveal possible talc-rich soils, as explained above for the komatiites. Except for the relatively high band 2 reflectance, giving the blue color to the dunite unit on Plate 2b, vegetation, although quite dense, appears not to dominate image color. Its main effect may be a lowering of apparent albedo through shading.

It is clear that the excellent empirical discrimination between basic and ultrabasic lithologies, with a very limited range of primary mineralogies, in the Marshall Pool area cannot be explained by direct reference to the primary mineralogical and geochemical differences between the rocks. It is due to variations in the proportions of a number of secondary compounds. In this small area, these remotely sensible conditions are consistently associated with units that would normally be distinguished on mineralogical and textural grounds only during intensive field mapping based on painstaking examination of float fragments and following poorly defined contacts, backed up by drilling. Even with detailed field mapping, the limited range of mineralogies in the lithologies considered often leads to misidentification without petrographic or geochemical study (Hallberg, 1986) and the overlooking of significant occurrences of important lithologies. Our work 100 km to the southeast in the Murrin-Margaret geological sector of the Laverton quadrangle (Hunt and Drury, *in prep.*) suggests that this consistency is widespread, at least for ultramafic and mafic units, and for terrains where erosion has breached and removed the lateritic duricrust. In areas where the thick lateritic cover remains largely intact, mapping by any means will always remain dependant on drilling alone. These parts of the Archaean terrain of the Yilgarn Block and other lateritized areas of basement form extremely important targets for gold, nickel, and platinoid-metal exploration. The results suggest that orperational Landsat Thematic Mapper data, suitably enhanced, will add significantly to the accuracy of geological mapping in both well-studied and sketchily mapped terrains in areas of deep, but breached, lateritic weathering. Prior to this, such terrains were regarded as unlikely to be amenable to reconnaissance mapping using operational satellite remote sensing, unlike the more ideal arid to semi-arid areas that have not undergone deep chemical weathering, which have dominated the literature of geological remote sensing hitherto.

ACKNOWLEDGMENTS

The work reported here was supported by an NERC Special Topic Research Contract (GST/02/125). The field work would not have been possible without provision of vehicles and bush kit by the Geological Survey of Western Australia (1985) and Esso Minerals Ltd (1986). Esso kindly loaned natural color aerial photographs of the study area. Dr. D.A. Rothery assisted in early field work.

REFERENCES

Abrams, M. J., J. E. Conel, and H. R. Lang, 1984. *The Joint NASA/Geosat Test Case Project: Final Report.* American Association of Petroleum Geologists, Tulsa, Oklahoma.

Bird, A. C., G. R. Garrard, A. R. Isles, C. A. Legg, W. P. Loughlin, and M. A. Tawfiq, 1985. An investigation of spectral signatures from mineralised rock outcrop, as defined by Airborne Thematic Mapper data of the Saudi Arabian Shield. *Proc. 3rd Int. Colloquium on Spectral Signatures of Objects in Remote Sensing: Les Arcs.* Remote Sensing Society/ISPRSC Commission VII, London.

Butt, C. R. M., 1981. The nature and origin of the laterite weathering mantle, with particular reference to Western Australia. *Geophysical Prospecting in Deeply Weathered Terrain.* (H. A. Doyle, J. E. Glover, and D. I. Groves, (Eds) Univ. Western Australia Geology Dept and Extension Service, Publ. 6, 11–29.

———, 1983. History and characteristics of weathering in Australia. *Geochemical Prospecting in Deeply Weathered Terrain.* CSIRO, Sydney, Australia, 41–50.

Canas, A. A. D., and M. E. Barnett, 1985. The generation and interpretation of false-colour principle component images. *Int. J. Remote Sensing*, 6, 867–81.

Donaldson, M. J., 1982. Mount Clifford - Marshall Pool area. *Regional Geology and Nickel Deposits of the Norseman-Wiluna Belt, Western Australia.* (D. I. Groves, and C. M. Lesher, (Eds)), University of Western Australia Geology Dept and Extension Service, Publ. 7, C53-67.

Fitzpatrick, E. A., 1980. *Soils, Their Formation and Distribution.* Longman, London, 353 p.

Gee, R. D., J. L. Baxter, S. A. Wilde, and I. R. Williams, 1981. Crustal development in the Archean Yilgarn Block, Western Australia. *Spec. Publ. Geol. Soc. Aust.*, 7, 43–56.

Gerstl, S. A. W. and C. Simmer, 1986. Radiation physics and modelling for off-nadir satellite sensing of non-Lambertian surfaces. *Remote Sensing of Environment*, 20, 1–30.

Gillespie, A. R., A. B. Kahle, and R. E. Walker, 1986. Color enhancement of highly correlated images - I. Decorrelation and HSI contrast stretches. *Remote Sensing of Environment*, 20, 209–35.

Graetz, R. D. and M. R. Gentle, 1982. The relationships between reflectance in the Landsat wavebands and the composition of an Australian semi-arid shrub rangeland. *Photogrammetric Engineering and Remote Sensing*, 11, 1721–30.

Hallberg, J. A., 1986. Archaean basin development and crustal extension in the northeastern Yilgarn Block, Western Australia. *Precambrian Res.*, 31, 133–56.

Hunt, G. A., S. A. Drury, and D. A. Rothery, 1986. Techniques for choosing the optimum TM channel combinations for lithological mapping in semi-arid terrains. *Proc. Int. Symp.: Mapping from Modern Imagery: Edinburgh*, Remote Sensing Society/ISPRS Commission VII, London, 637–46.

Hunt, G. R. and C. E. Russell, 1981. The use of near-infrared spectroscopy to determine the degree of serpentinization of ultramafic rocks. *Geophysics*, 46, 316–21.

McFarlane, M. J., 1976. *Laterite and Landscape*, Academic Press, London.

Ollier, C. D., 1978. Early landform evolution. *Australia, a Geography*, (J. N. Jeans, (Ed.)) Sydney University Press, Sydney, 85–98.

Podwysocki, M.H., D. B. Segal, and M. J. Abrams, 1983. Use of multispectral scanner images for assessment of hydrothermal alteration in the Marysville, Utah, mining district. *Econ. Geol.*, 78, 675–87.

Sheffield, C., 1985. Selecting band combinations from multispectral data. *Photogrammetric Engineering and Remote Sensing*, 51, 681–7.

Smith, B. H., 1977. Some aspects of the use of geochemistry in the search for nickel sulphides in lateritic terrain in Western Australia. *J. Geochem. Explor.*, 8, 259–81.

Soha, J. H., and A. A. Schwartz, 1978. Multispectral histogram normalization and contrast enhancement. *Proc. 5th Canadian Symp. on Remote Sensing*, 86–103.

Sultan, M., R. Arvidson, N. Sturchio, and E. A. Guinness, 1987. Lithological mapping in arid regions with Landsat Thematic Mapper data: Meatiq Dome, Egypt. *Geol. Soc. Amer. Bull.*, 99, 748–62.

Thom, R., and R. G. Barnes, 1977. Leonora, Western Australia. *Geological Survey of Western Australia, 1: 250 000 Geol. Series — Explanatory Notes*, SH/51-1.

(Received 21 October 1987; accepted 17 February 1988; revised April 1988)